Qiu et al. *Zool. Res.* 2024, 45(3): 679−690
https://doi.org/10.24272/j.issn.2095-8137.2023.302

ZR | Zoological Research

Article Open Access

In vivo imaging reveals a synchronized correlation among neurotransmitter dynamics during propofol and sevoflurane anesthesia

Gao-Lin Qiu[1,#], Li-Jun Peng[1,#], Peng Wang[1,#], Zhi-Lai Yang[1], Ji-Qian Zhang[1], Hu Liu[1], Xiao-Na Zhu[2,*], Jin Rao[1,*], Xue-Sheng Liu[1,*]

[1] *Department of Anesthesiology*, *First Affiliated Hospital of Anhui Medical University*, *Hefei*, *Anhui* 230022, *China*
[2] *School of Life Science and Technology*, *ShanghaiTech University*, *Shanghai* 201210, *China*

ABSTRACT

General anesthesia is widely applied in clinical practice. However, the precise mechanism of loss of consciousness induced by general anesthetics remains unknown. Here, we measured the dynamics of five neurotransmitters, including γ-aminobutyric acid, glutamate, norepinephrine, acetylcholine, and dopamine, in the medial prefrontal cortex and primary visual cortex of C57BL/6 mice through *in vivo* fiber photometry and genetically encoded neurotransmitter sensors under anesthesia to reveal the mechanism of general anesthesia from a neurotransmitter perspective. Results revealed that the concentrations of γ-aminobutyric acid, glutamate, norepinephrine, and acetylcholine increased in the cortex during propofol-induced loss of consciousness. Dopamine levels did not change following the hypnotic dose of propofol but increased significantly following surgical doses of propofol anesthesia. Notably, the concentrations of the five neurotransmitters generally decreased during sevoflurane-induced loss of consciousness. Furthermore, the neurotransmitter dynamic networks were not synchronized in the non-anesthesia groups but were highly synchronized in the anesthetic groups. These findings suggest that neurotransmitter dynamic network synchronization may cause anesthetic-induced loss of consciousness.

Keywords: General anesthesia; Loss of consciousness; *In vivo* neurotransmitter imaging; Medial prefrontal cortex; Primary visual cortex

INTRODUCTION

Each year, worldwide, at least 320 million patients undergoing surgery benefit from the unique ability of general anesthetics to induce safe and reversible loss of consciousness (LOC) (Rose et al., 2015). Despite this, the mechanisms underlying anesthetic-induced LOC (aLOC) remain elusive (Hudetz & Mashour, 2016; Meyer, 2015). Previous studies have focused on the effect of anesthetics on functional connectivity within the cortical network (Alkire et al., 2008; Barttfeld et al., 2015; Luppi et al., 2019; Supp et al., 2011). Elucidating the dynamics of neuronal communication, mainly mediated by neurotransmitters, is needed to understand the precise functional connections within the cortical network during aLOC (Fornito et al., 2015). In the past, neurotransmitters have been detected through *ex vivo* electrophysiology of receptor-mediated currents, *in vivo* microdialysis, and fast-scan cyclic voltammetry (FSCV). However, the extent to which *ex vivo* electrophysiology alone can accurately reflect the true sensitivity of living organisms remains uncertain. Moreover, the spatiotemporal precision of microdialysis is deemed insufficient, and neurotransmitters with similar structures cannot be effectively distinguished using FSCV (Sun et al., 2018). In response to these limitations, recent developments in genetically encoded, fluorescent neurotransmitter sensors have revolutionized the detection of concentration changes in neurotransmitters in the brain with high spatiotemporal resolution and specificity, with successful application in freely moving mice (Guo et al., 2021; Wang et al., 2018).

The medial prefrontal cortex (mPFC) plays a pivotal role in conscious experience (Carhart-Harris et al., 2012; Silva et al., 2015). Studies have also implicated the mPFC as a potentially important target area for general anesthetics to induce LOC by affecting information integration in the brain (Leon-Dominguez et al., 2014; Smith et al., 2017; Wang et al., 2016). The mPFC network is mainly composed of excitatory pyramidal neurons and inhibitory interneurons (Xu et al., 2019), which form a complex network through synaptic interconnections and the

Received: 12 November 2023; Accepted: 25 December 2023; Online: 26 December 2023
Foundation items: This work was supported by the National Natural Science Foundation of China (81870841 and 82171192 to X.S.L., 82101349 to G.L.Q.)
[#]Authors contributed equally to this work
*Corresponding authors, E-mail: zhuxn@shanghaitech.edu.cn; 18256954080@163.com; liuxuesheng@ahmu.edu.cn

release of various neurotransmitters. Suppression of excitatory synaptic transmission and facilitation of inhibitory synaptic transmission are posited as possible mechanisms underlying aLOC (Hemmings et al., 2005; Liu et al., 2020). Therefore, accurate dissection of neurotransmitter transients and neural functions in the mPFC under general anesthesia may be crucial for elucidating aLOC. Nevertheless, neurotransmitter detection in the mPFC under anesthesia has traditionally been restricted to one or two types, with the technology used for detection showing deficiencies in prior studies (Müller et al., 2011).

In addition, the primary visual cortex (V1), which plays an important role in the maintenance of consciousness (Guo et al., 2021), has also been studied to explore whether neurotransmitter changes induced by anesthesia are local or global.

Thus, we conducted a comprehensive study to investigate how exposure to propofol or sevoflurane modulates the concentration of five excitatory and inhibitory neurotransmitters, including γ-aminobutyric acid (GABA), glutamate (Glu), norepinephrine (NE), acetylcholine (ACh), and dopamine (DA), in the mPFC and V1 using fiber photometry and neurotransmitter sensors. Results revealed that the neurotransmitter dynamics in the mPFC and V1 regions displayed a disorganized response pattern during aLOC. Through correlation analysis, we determined that neurotransmitter dynamic network synchronization may represent a common mechanism of aLOC.

MATERIALS AND METHODS

Ethics statement

All applicable international, national, and institutional guidelines for the care and use of animals were strictly followed. All animal sample collection protocols complied with the current laws of China. All animal procedures performed in this research were conducted in accordance with the ethical standards of the institution or organization where the study was conducted (Standing Committee on Animals of Anhui Medical University (protocol number: LLSC20211529)).

Animals

Healthy male C57BL/6 mice (2–4 months, 22–28 g) were purchased from the SLAC Laboratory Animal Center (Shanghai, China). All mice were maintained on a 12 h day/12 h night cycle at a constant temperature (24±2°C) and humidity (55%±5%), with food and water provided *ad libitum*. All mice were randomly assigned to each group.

Drugs

Isoflurane (RWD Life Science, China) was administered at concentrations of 4% and 1.5% for anesthesia induction and maintenance, respectively. Additionally, propofol (Corden Pharma S.P.A., Italy) was intraperitoneally (i.p.) injected at doses of 25, 100, and 200 mg/kg. Sevoflurane (Hearem, China) was administered at doses of 0.3%, 3%, and 5%. The time interval between administering different concentrations of anesthesia to the same mouse was 5 days.

Adeno-associated virus (AAV) vectors

AAV vectors containing hSyn-DA3m (Sun et al., 2020), hSyn-iGABASnFR (Marvin et al., 2019), hSyn-iGluSnFR (A184S) (Marvin et al., 2018), hSyn-ACh3.0 (Jing et al., 2020), and hSyn-GRAB-NE2m (3.1) (Feng et al., 2019) were packaged into the AAV2/9 serotype with titers of 1–5×10^{12} viral particles per mL. The rAAVs were purchased from Brain VTA (China), with all reporters validated for use with fiber photometry (Feng et al., 2019; Jing et al., 2020; McGovern et al., 2021; Sun et al., 2020; Zheng et al., 2020).

Virus injection and optical fiber implantation

The surgical procedure was similar to that described by our previous research (Qiu et al., 2020). Briefly, anesthesia was induced at 4% and maintained with 1.5% of isoflurane. The mice were then placed in a stereotaxic instrument (RWD Life Science, China) to adjust their skulls parallel to the reference panel, after which a small hole was gently drilled into the skull. Using a microsyringe pump (RWD Life Science, China), 300 nL of rAAV was slowly injected for 5 min through a sharp glass pipette into the mPFC (coordinates from bregma: 1.6 mm anteroposterior (AP), ±0.3 mm mediolateral (ML), −1.9 mm dorsoventral (DV)) or the V1 (−2.5 mm AP, ±2.5 mm ML, −0.5 mm DV). The glass pipette was kept still for at least 15 min after the injection. A cannula-bound optical fiber (200 μm O.D., 0.39 NA, RWD Life Science, China) was immediately implanted with the tip positioned 20 μm above the injection sites, then secured using Super-Bond C&B dental acrylic (NISSIN, Japan). After the dental cement had completely dried, the mice were removed from the stereotaxic instrument and placed on an electric blanket to be kept warm (37°C) until full recovery, at which point they were returned to their home cages. The virus injection sites and precise locations of the optical fiber in the stereotaxic atlas are displayed in Supplementary Figure S1 A–D.

Fiber photometry

After recovering from surgery for 2–3 weeks, the mice underwent fiber photometry recordings following 30 min of acclimatization to the test environment (Figure 1A). After anesthetizing mice with propofol or sevoflurane, their rectal temperatures were monitored (Wi78653, Dongxi Instrument, China). The temperature in the anesthesia chamber was maintained at 37±1°C by positioning a warming pad beneath a transparent gas-tight chamber. The chamber featured connections on the left and right for oxygen input and output. The mice breathed spontaneously, and the concentrations of anesthetic, oxygen, and carbon dioxide were continuously monitored using a calibrated Datex-Ohmeda gas analyzer (GE Healthcare, USA).The connections were attached to an oxygen generator (Hong Xinyuan Electronics, China) and an animal anesthesia volatilization tank (Sevotec5, Ohmeda, USA), with oxygen supplied at a fixed flow rate of 1 L/min. To minimize errors associated with i.p. injections of propofol, extensive practice sessions preceded the formal experiment. In our experiments, all mice treated with propofol (100 mg/kg, 200 mg/kg) developed a loss of righting reflex (LORR). Subsequently, fluorescence signals were recorded using light-emitting diodes (480 nm, 405 nm, Lumileds, China) reflected by a dichroic mirror (Edmund Optics, USA) and focused through an objective lens (20×, NA0.4, Olympus, Japan). The laser power was adjusted to 40–70 μW to minimize bleaching. Fluorescence emissions were bandpass filtered (87753, Edmund Optics, USA), and detected by a photomultiplier tube (H10721, Hamamatsu, Japan). An amplifier was used to convert the photomultiplier tube current output to voltage, which was further filtered through a low-pass filter (35 Hz cut-off, ThinkerTech, China). The analog voltage signals were digitalized at 100 Hz and recorded using fiber photometry

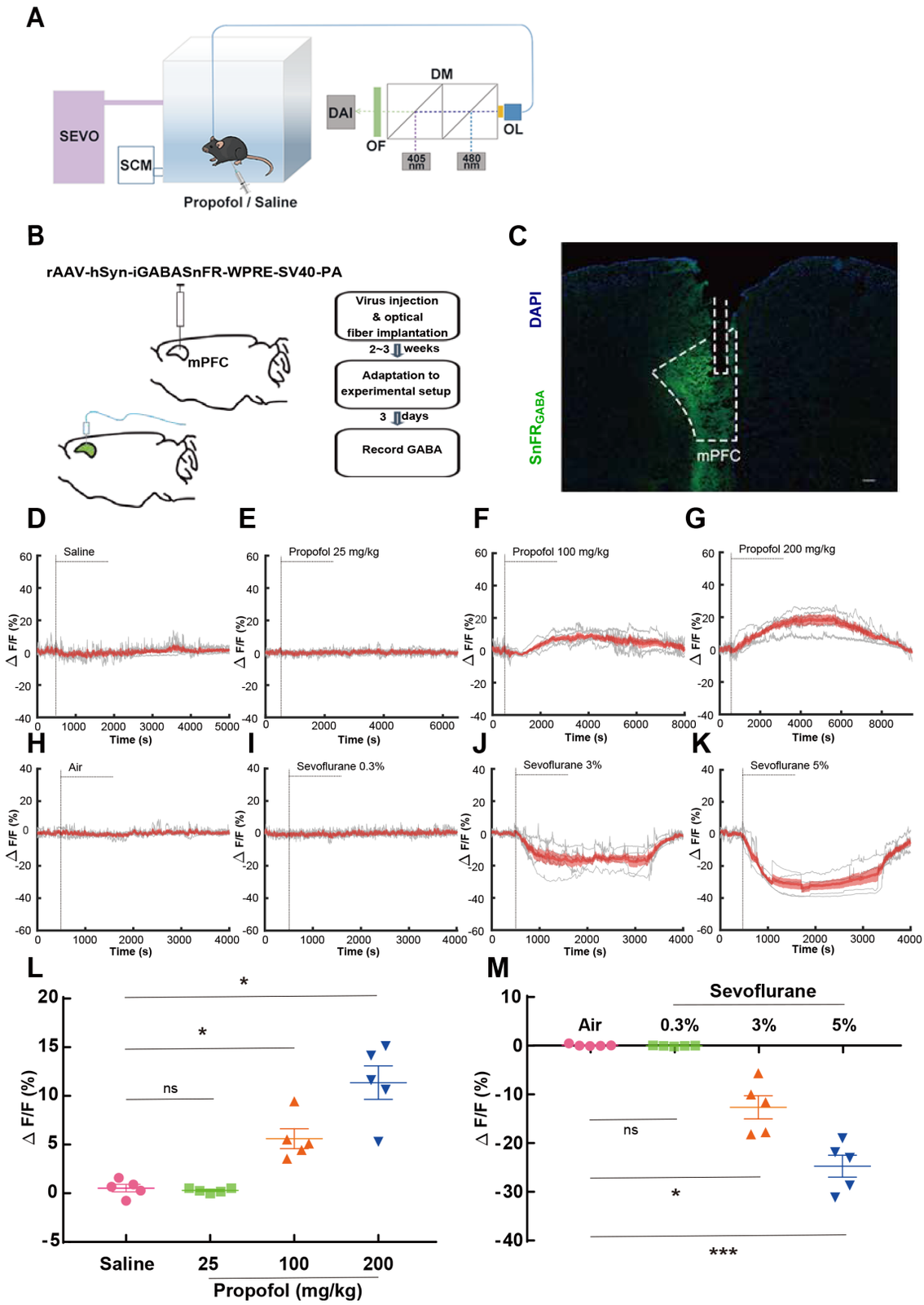

Figure 1 Propofol increases and sevoflurane decreases GABA in the mPFC

A: Schematic of experimental setup used for fiber photometry to detect fluorescence changes in freely behaving mice following drug administration. B: Experimental strategy to record GABA signal changes in mPFC neurons using fiber photometry. C: Representative image displaying GABA sensor and fiber channel in the mPFC sample. Scale bar: 200 μm. D−K: GABA signals in the mPFC of five mice individually challenged with saline, propofol (25, 100, or 200 mg/kg), air, and sevoflurane (0.3%, 3%, or 5%) administration. Vertical dashed line indicates start of administration. Gray lines depict signals from each mouse, with mean values represented by a red line and SEM intervals shaded in red (n=5 mice). L−M: Statistical results of GABA signal changes (one-way ANOVA followed by Dunnett's *post hoc* test; error bars indicate SEM). *: P<0.05; **: P<0.01; ***: P<0.001; ns, not significant. SEVO, sevoflurane; SCM, sevoflurane concentration monitor; DAI, data acquisition interface; OF, optical filter; OL, objective lens; DM, dichroic mirror.

software (ThinkerTech, China). Before the administration of anesthesia, saline, or air, each mouse was connected to the optical fiber recording system and allowed to move freely. When anesthesia, saline, or air was administered, the time was recorded, and fiber recordings were continued until the mouse fully recovered from the anesthesia or reached the equivalent time of anesthesia. LORR was defined as the loss of consciousness, marked by the disappearance of righting reflex, and observed when the mice were lying flat and unable to turn over and touch the ground on all fours. Data from the entire optical fiber recording process were collected for processing. After recording, the photometry data were exported to mat. files. The values of fluorescence change (ΔF/F), defined as (F−F0)/F0, were then calculated, with F0 representing the baseline fluorescence signal averaged over a 110 s control time window. The ΔF/F values were visualized as red average plots, with gray curves representing trial-by-trial signal changes. The data were initially segmented based on behavioral events, and average calcium signals were then calculated after saline, propofol, or sevoflurane administration. Notably, when an extracellular neurotransmitter increases, the neurotransmitter interacts with the probe expressed on the neuron, causing the probe to expose more fluorescent protein, resulting in an enhanced fluorescence signal. Therefore, an increase in the fluorescence signal values indicated that the concentration of the neurotransmitter had increased, and vice versa.

Electroencephalogram (EEG) recording and analysis

The EEG recording and analysis procedures closely followed our prior research (Qiu et al., 2020). After anesthetization via an i.p. injection of pentobarbital (50 mg/kg), the mice were placed on the stereotaxic positioning instrument and kept warm (37°C) with an electric heating pad. Three holes were drilled with a carbide bit: one over the left frontal cortical area (1 mm anterior to bregma, 1.5 mm lateral to midline), one over the parietal area (1 mm anterior to lambda, 1.5 mm lateral to midline) of the right hemisphere, and one over the parietal area (1 mm anterior to lambda, 1.5 mm lateral to midline) of the left hemisphere. Three electrodes were then implanted in the holes and fixed with dental cement. After the dental cement had completely dried, the mice were removed from the stereotaxic instrument and placed on an electric blanket, before being returned to their home cage upon complete recovery. EEG recordings were conducted 14 days after surgery. The EEG data were digitized at 1 kHz using the PowerLab and LabChart system (AD Instruments, New Zealand), low-pass filtered at 50 Hz, and high-pass filtered at 0.3 Hz. The power spectrum between 0.1 and 30 Hz was transformed using the “mtspecgramc” function in the MATLAB signal processing toolbox chronux_2_12 (MathWorks, USA).

Histology

After deep anesthesia by an i.p. injection of pentobarbital (100 mg/kg), the mice were transcardially perfused with saline to remove the blood, followed by perfusion with 4% paraformaldehyde (PFA) to fix the brain. Their heads were removed and soaked in 4% PFA at 4°C overnight, after which the brains were immersed in 30% sucrose in phosphate-buffered saline (PBS, 0.1 mol/L, pH 7.4) at 4°C for 24 h. Coronal sections (20 μm) containing the mPFC, V1, and optical fiber position were sliced using a cryostat (Leica MNT21001, Germany). The slides were thoroughly washed with PBS and stained with 1:10 diluted 4’,6-diamidino-2-phenylindole (DAPI) for 5 min to identify cell bodies. After washing with PBS, 10% glycerin was used to seal the slides. Finally, fluorescent images were collected using a TissueFAXS system (TissueGnostics, Austria).

Statistical analyses

The mice were randomly assigned to the treatment groups using the random number table method, and mice in each group were tested in ascending order. No missing data occurred for the variables, and no outliers were present. All statistical analyses were performed using SPSS v.23.0 (GraphPad Software, USA) or MATLAB R2020a (MathWorks, USA). Differences between two groups were analyzed using paired *t*-tests, while differences among more than two groups were analyzed using one-way analysis of variance (ANOVA) followed by Dunnett’s *post hoc* test. Pearson pairwise correlation coefficient (Pearson’s *r*) was employed to analyze data significance and correlation. In all cases, statistical significance was set at $P<0.05$. Asterisks denote statistical significance at $^{*}P<0.05$, $^{**}P<0.01$, and $^{***}P<0.001$. Unless otherwise indicated, data are expressed as mean (standard error of the mean (SEM)). An absolute value of $r>0.4$ was denoted as a high correlation.

RESULTS

Propofol increases and sevoflurane decreases GABA

To systematically monitor neurotransmitter transmission dynamics in the mPFC and V1 during aLOC with high spatiotemporal resolution, we employed *in vivo* fiber photometry to record responses during propofol and sevoflurane anesthesia (Figure 1A). We first examined the effects of propofol and sevoflurane on the most representative inhibitory neurotransmitter, GABA, involving viral hSyn-iGABASnFR stereotaxic injection and optical fiber implantation in the mPFC and V1 of C57BL/6 mice (Figure 1B, C; Supplementary Figure S2A, B). After 2–3 weeks of recovery and 3 days of adaptation, the mice were placed in an operant box, and fiber photometry was performed to monitor changes in GABA sensor fluorescence in response to i.p. injection of saline (10 μL/g) or 2% propofol (25, 100, or 200 mg/kg) (Irifune et al., 2003; Liu et al., 2016; Patel et al., 2003) or inhalation of air or sevoflurane (0.3%, 3%, or 5%) (Alkire & Gorski, 2004; Nishino et al., 2020; Zhou et al., 2015). Extracellular GABA was quantified as the fluorescence intensity of green fluorescent protein (GFP). In the propofol (100 and 200 mg/kg) and sevoflurane (3% and 5%) groups, all mice entered the LORR state (LOC). Changes in neurotransmitter levels coincided with the onset of LOC. GABA activity was dynamic during propofol and sevoflurane-induced LOC, indicating the technical feasibility of GABA imaging. We observed that the GABA concentration did not change when saline (Figure 1D; Supplementary Figure S2C), low-dose propofol (25 mg/kg, Figure 1E), air (Figure 1H; Supplementary Figure S2F), or low-dose sevoflurane (0.3%, Figure 1I) were administered in the mPFC and V1. Conversely, the GABA concentration significantly increased with the administration of hypnotic (100 mg/kg, Figure 1F; Supplementary Figure S2D) and surgical doses of propofol (200 mg/kg, Figure 1G), but significantly decreased with the administration of hypnotic (3%, Figure 1J; Supplementary Figure S2G) and surgical doses of sevoflurane (5%, Figure 1K). Analyses demonstrated that acute propofol

exposure led to a sustained increase in GABA levels in a dose-dependent manner (F=27.86, P=0.0008, Figure 1L; saline, −0.07 (−0.32; 0.43), median (25%; 75%) vs. propofol, 4.96 (4.51; 6.47), P=0.0006, Supplementary Figure S2E). Conversely, acute sevoflurane exposure caused a significant dose-dependent decrease in GABA (F=54.02, P<0.0001, Figure 1M; air, 0.11 (−0.22; 0.32), median (25%; 75%) vs. sevoflurane, −11.12 (−15.45; −8.95), P=0.006, Supplementary Figure S2H).

Propofol increases and sevoflurane decreases Glu

Next, we investigated the effects of propofol and sevoflurane on the most representative excitatory neurotransmitter, Glu, involving viral hSyn-iGluSnFR (A184S) stereotaxic injections and optical fiber implantation in the mPFC and V1 of C57BL/6 mice (Figure 2A, B; Supplementary Figure S3A, B). After 2–3 weeks of recovery and 3 days of adaptation, the mice were placed in an operant box, and fiber photometry was performed to monitor changes in Glu sensor fluorescence in response to i.p. injection of saline (10 μL/g) or 2% propofol (25, 100, or 200 mg/kg) or inhalation of air or sevoflurane (0.3%, 3%, or 5%). Extracellular Glu was quantified as the fluorescence intensity of GFP. In the propofol (100 and 200 mg/kg) and sevoflurane (3% and 5%) groups, all mice entered the LORR state (LOC). Changes in neurotransmitter levels coincided with the onset of LOC. Glu activity was dynamic during propofol and sevoflurane-induced LOC, indicating the technical feasibility of Glu imaging. The Glu concentration did not change when saline (Figure 2C; Supplementary Figure S3C), low-dose propofol (25 mg/kg, Figure 2D), air (Figure 2G; Supplementary Figure S3F), or low-dose sevoflurane (0.3%, Figure 2H) were administered in the mPFC and V1. However, the Glu concentration significantly increased upon administration of hypnotic (100 mg/kg, Figure 2E; Supplementary Figure S3D) and surgical doses of propofol (200 mg/kg, Figure 2F) and significantly decreased during the administration of hypnotic (3%, Figure 2I; Supplementary Figure S3G) and surgical doses of sevoflurane (5%, Figure 2J). Analyses demonstrated that acute propofol exposure led to a significant dose-dependent increase in Glu (F=54.36, P=0.0003, Figure 2K; saline,0.18 (0.05; 0.21), median (25%; 75%) vs. propofol, 3.43 (2.77; 4.89), P=0.005, Supplementary Figure S3E), while acute sevoflurane exposure led to significant dose-dependent decrease in Glu (F=15.07, P=0.011, Figure 2L; air, −0.05 (−0.33; 0.11), median (25%; 75%) vs. sevoflurane, −6.72 (−10.59; −6.57), P=0.005, Supplementary Figure S3H).

Propofol increases and sevoflurane decreases NE

We next explored the effects of propofol or sevoflurane treatment on the excitatory neurotransmitter NE, involving viral hSyn-GRAB-NE2m (3.1) stereotaxic injections and optical fiber implantation in the mPFC and V1 of C57BL/6 mice (Figure 3A, B; Supplementary Figure S4A, B). After 2–3 weeks of recovery and 3 days of adaptation, the mice were placed in an operant box, and fiber photometry was performed to monitor changes in NE sensor fluorescence in response to i.p. injection of saline (10 μL/g) or 2% propofol (25, 100, or 200 mg/kg) or inhalation of air or sevoflurane (0.3%, 3%, or 5%). Extracellular NE was quantified by the fluorescence intensity of GFP. In the propofol (100 and 200 mg/kg) and sevoflurane (3% and 5%) groups, all mice entered the LORR state (LOC). Changes in neurotransmitter levels coincided with the onset of LOC. NE activity was dynamic during propofol and sevoflurane-induced LOC, indicating the technical feasibility of NE imaging. The NE concentration did not change when saline (Figure 3C; Supplementary Figure S4C), low-dose propofol (25 mg/kg, Figure 3D), air (Figure 3G; Supplementary Figure S4F), or low-dose sevoflurane (0.3%, Figure 3H) were administered in the mPFC and V1. However, the NE concentration significantly increased upon administration of hypnotic (100 mg/kg, Figure 3E; Supplementary Figure S4D) and surgical doses of propofol (200 mg/kg, Figure 3F) and significantly decreased upon administration of hypnotic (3%, Figure 3I; Supplementary Figure S4G) and surgical doses of sevoflurane (5%, Figure 3J). Analyses indicated that acute propofol exposure led to a marked dose-dependent increase in NE (F=28.88, P=0.0003, Figure 3K; saline, 0.02 (−0.08; 0.11), median (25%; 75%) vs. propofol, 8.48 (7.11; 12.49), P=0.004, Supplementary Figure S4E), while acute sevoflurane exposure caused a significant dose-dependent decrease in NE (F=28.52, P=0.003, Figure 3L; air, −0.14 (−0.49; −0.10), median (25%; 75%) vs. sevoflurane, −0.94 (−10.38; −4.50), P=0.010, Supplementary Figure S4H).

Propofol increases and sevoflurane decreases ACh

We next explored changes in the excitatory neurotransmitter ACh, involving viral hSyn-ACh3.0 stereotaxic injections and optical fiber implantation in the mPFC and V1 of C57BL/6 mice (Figure 4A, B; Supplementary Figure S5A, B). After 2–3 weeks of recovery and 3 days of adaptation, the mice were placed in an operant box, and fiber photometry was performed to monitor changes in ACh sensor fluorescence in response to i.p. injection of saline (10 μL/g) or 2% propofol (25, 100, or 200 mg/kg) or inhalation of air or sevoflurane (0.3%, 3%, or 5%). Extracellular ACh was quantified as the fluorescence intensity of GFP. In the propofol (100 and 200 mg/kg) and sevoflurane (3% and 5%) groups, all mice entered the LORR state (LOC). Changes in neurotransmitter levels coincided with the onset of LOC. ACh activity was dynamic during propofol and sevoflurane-induced LOC, indicating the technical feasibility of ACh imaging. The ACh concentration did not change when saline (Figure 4C; Supplementary Figure S5C), low-dose propofol (25 mg/kg, Figure 4D), air (Figure 4G; Supplementary Figure S5F), or low-dose sevoflurane (0.3%, Figure 4H) were administered in the mPFC and V1. However, its concentration significantly increased upon administration of hypnotic (100 mg/kg, Figure 4E; Supplementary Figure S5D) and surgical doses of propofol (200 mg/kg, Figure 4F) and significantly decreased upon administration of hypnotic (3%, Figure 4I; Supplementary Figure S5G) and surgical doses of sevoflurane (5%, Figure 4J). Analyses demonstrated that acute propofol exposure led to a sustained dose-dependent increase in ACh (F=15.05, P=0.011, Figure 4K; saline, −0.01 (−0.03; 0.04), median (25%; 75%) vs. propofol, 5.49 (3.55; 9.24), P=0.01, Supplementary Figure S5E); however, acute sevoflurane exposure resulted in a significant dose-dependent decrease in ACh (F=24.56, P=0.001, Figure 4L; air, −0.13 (−0.60; 0.40), median (25%; 75%) vs. sevoflurane, −4.66 (−12.09; −4.24), P=0.025, Supplementary Figure S5H).

Propofol increases and sevoflurane decreases DA

Finally, we explored the excitatory neurotransmitter DA, involving viral hSyn-DA3m stereotaxic injections and optical fiber implantation in the mPFC and V1 of C57BL/6 mice

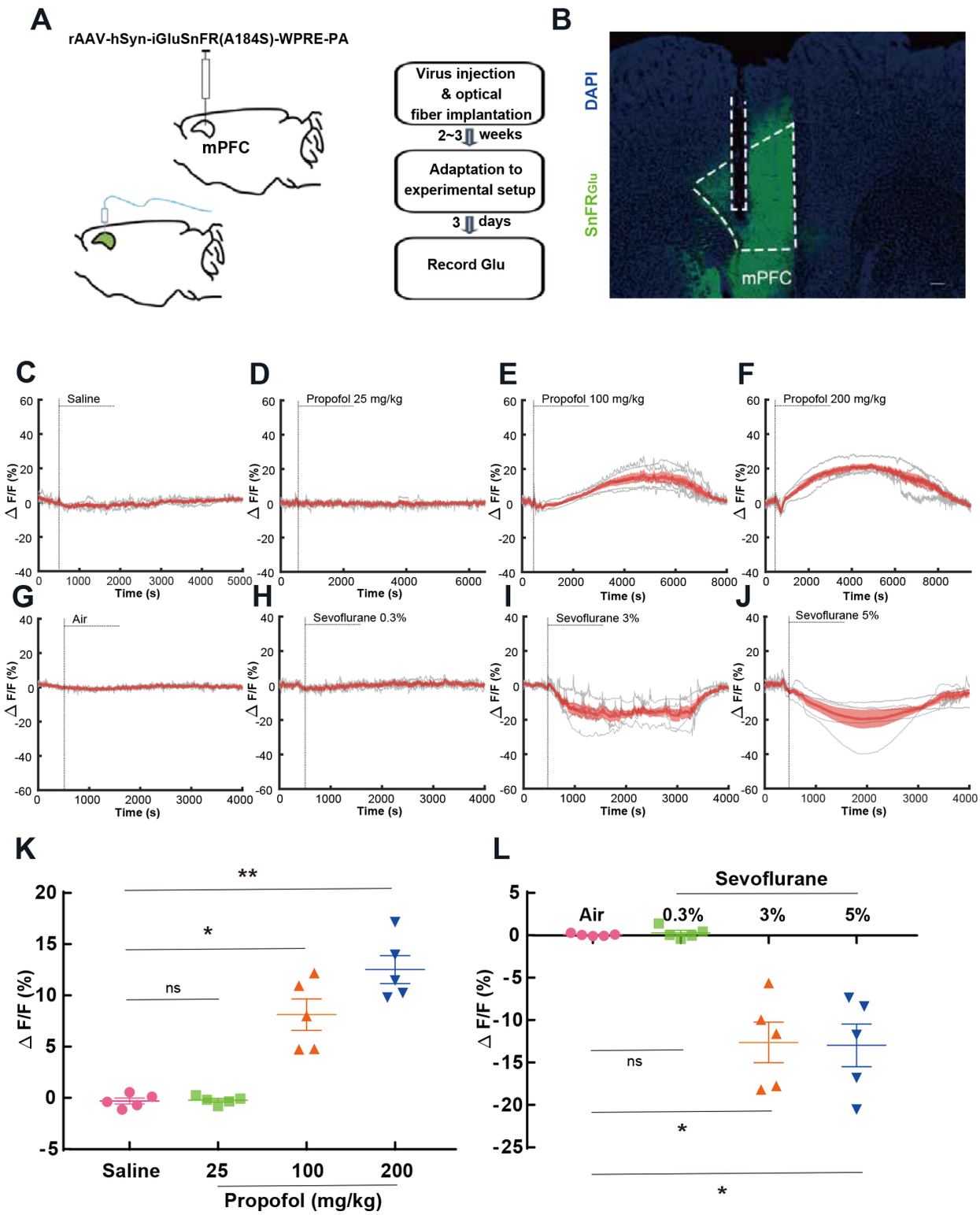

Figure 2 Propofol increases and sevoflurane decreases Glu in the mPFC

A: Experimental strategy used to record changes in Glu signals from mPFC neurons using fiber photometry. B: Representative image displaying Glu sensor and fiber channel in the mPFC sample. Scale bar: 200 μm. C–J: Glu signals in the mPFC of five mice individually challenged with saline, propofol (25, 100, or 200 mg/kg), air, and sevoflurane (0.3%, 3%, or 5%) administration. Vertical dashed line indicates start of administration. Gray lines depict signals from each mouse, with mean values represented by a red line and SEM intervals shaded in red (n=5 mice). K, L: Statistical results of Glu signal changes (one-way ANOVA followed by Dunnett's *post hoc* test; error bars indicate SEM). *: P<0.05; **: P<0.01; ***: P<0.001; ns, not significant.

(Figure 5A, B; Supplementary Figure S6A, B). After 2–3 weeks of recovery and 3 days of adaptation, the mice were placed in an operant box, and fiber photometry was performed to monitor changes in DA sensor fluorescence in response to i.p. injection of saline (10 μL/g) or 2% propofol (25, 100, or 200 mg/kg) or inhalation of air or sevoflurane (0.3%, 3%, or

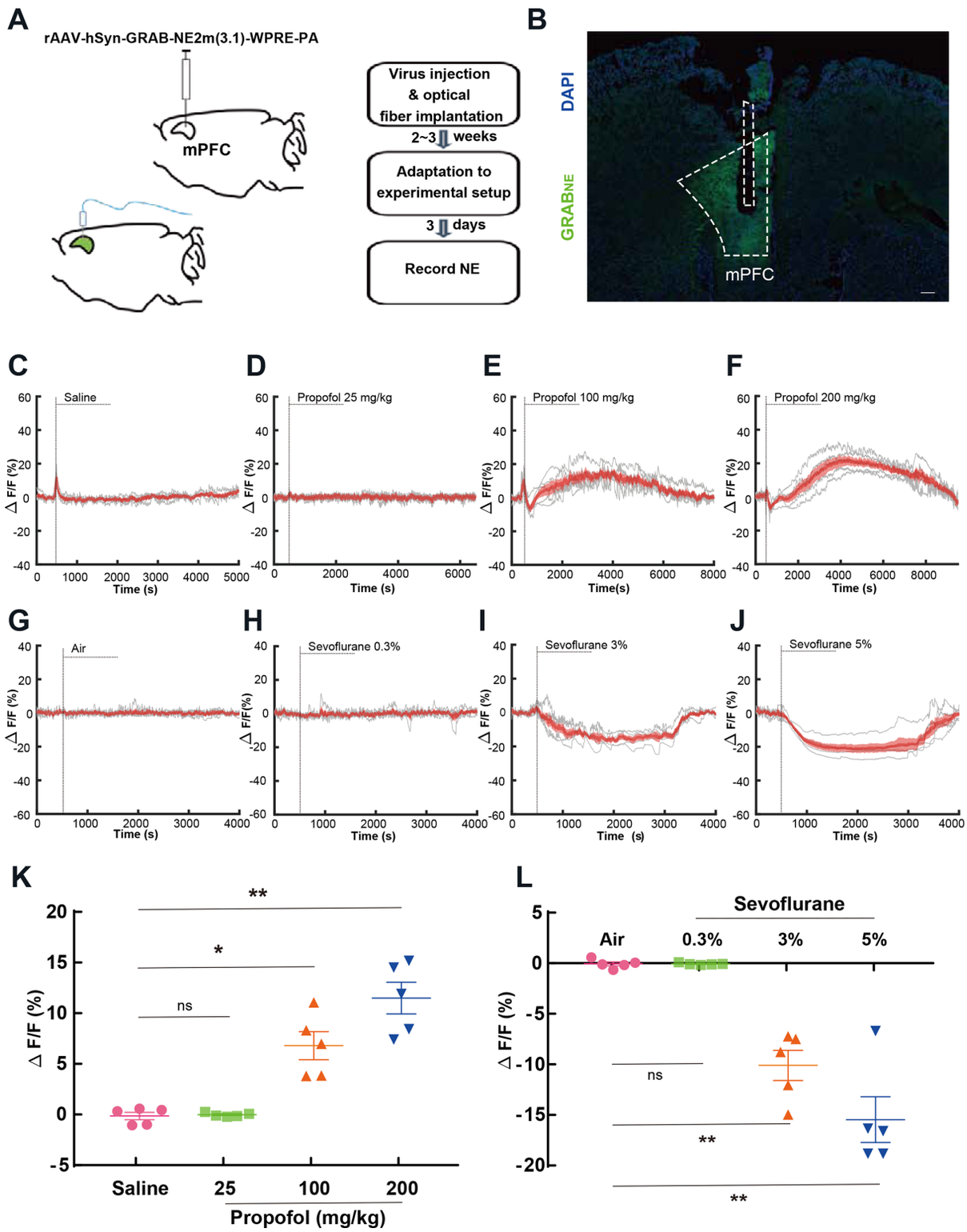

Figure 3 Propofol increases and sevoflurane decreases NE in the mPFC

A: Experimental strategy to record changes in NE signals from mPFC neurons using fiber photometry. B: Representative image displaying NE sensor and fiber channel in the mPFC sample. Scale bar: 200 μm. C−J: NE signals in the mPFC of five mice individually challenged with saline, propofol (25, 100, or 200 mg/kg), air, and sevoflurane (0.3%, 3%, or 5%) administration. Vertical dashed line indicates start of administration. Gray lines depict signals from each mouse, with mean values represented by a red line and SEM intervals shaded in red (*n*=5 mice). K, L: Statistical results of NE signal changes (one-way ANOVA followed by Dunnett's *post hoc* test; error bars indicate SEM). *: $P<0.05$; **: $P<0.01$; ***: $P<0.001$; ns, not significant.

5%). Extracellular DA was quantified as the fluorescence intensity of GFP. In the propofol (100 and 200 mg/kg) and sevoflurane (3%, 5%) groups, all mice entered the LORR state (LOC). Changes in neurotransmitter levels coincided with the onset of LOC. The DA activity was dynamic during propofol and sevoflurane-induced LOC, indicating the technical

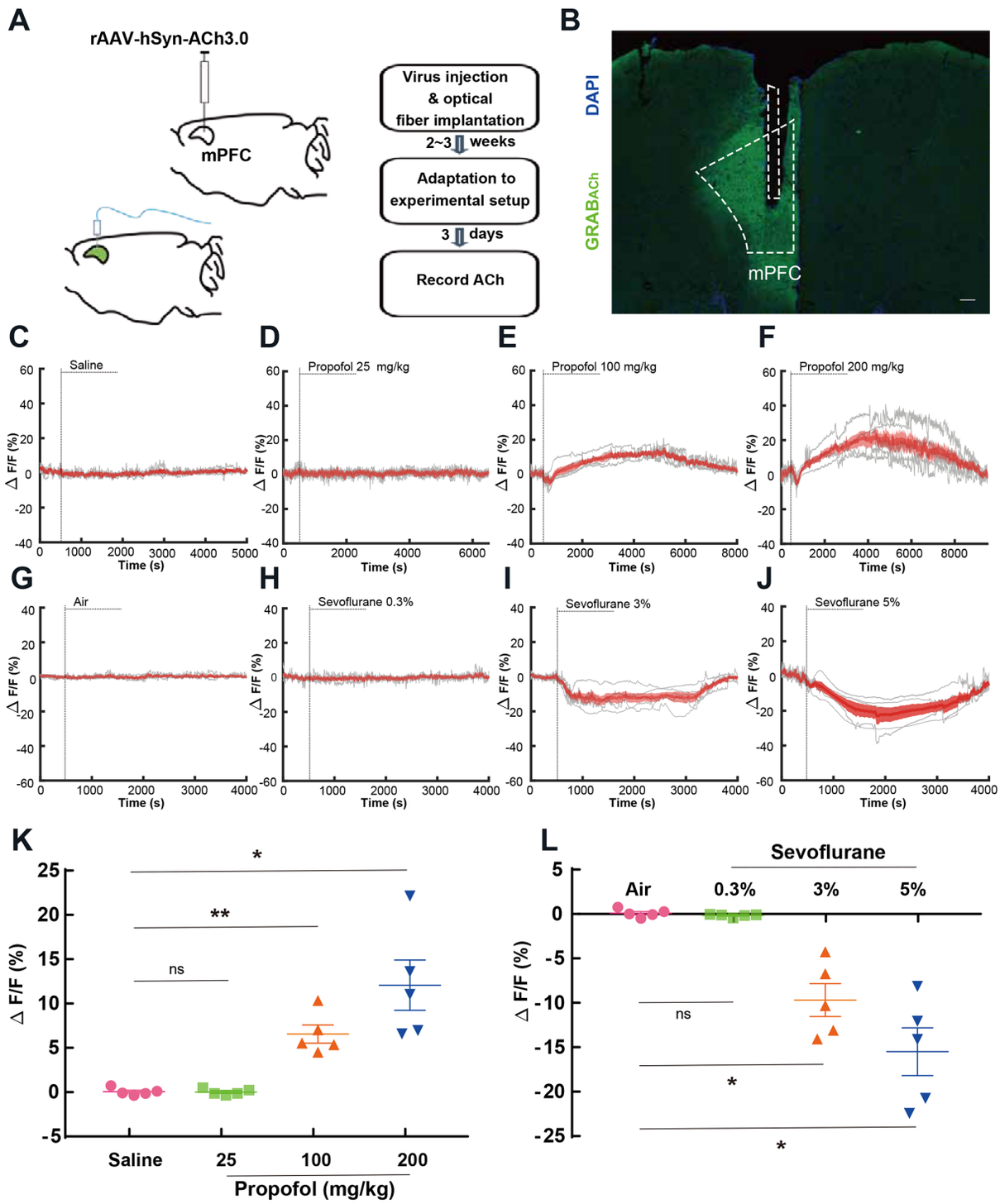

Figure 4 Propofol increases and sevoflurane decreases ACh in the mPFC

A: Experimental strategy to record changes in ACh signals from mPFC neurons using fiber photometry. B: Representative image displaying ACh sensor and fiber channel in the mPFC sample. Scale bar: 200 μm. C−J: ACh signals in the mPFC of five mice individually challenged with saline, propofol (25, 100, or 200 mg/kg), air, and sevoflurane (0.3%, 3%, or 5%) administration. Vertical dashed line indicates start of administration. Gray lines depict signals from each mouse, with mean values represented by a red line and SEM intervals shaded in red (n=5 mice). K, L: Statistical results of ACh signal changes (one-way ANOVA followed by Dunnett's *post hoc* test; error bars indicate SEM). *: P<0.05; **: P<0.01; ***: P<0.001; ns, not significant.

feasibility of DA imaging. The DA concentration did not change when saline (Figure 5C; Supplementary Figure S6C), low-dose propofol (25 mg/kg, Figure 5D), hypnotic doses of propofol (100 mg/kg, Figure 5E; Supplementary Figure S6D), air (Figure 5G; Supplementary Figure S6F), or low-dose sevoflurane (0.3%, Figure 5H) were administered in the mPFC and V1. However, DA concentration was elevated upon administration of surgical doses of propofol (200 mg/kg, Figure 5F) and significantly decreased upon administration of hypnotic (3%, Figure 5I; Supplementary Figure S6G) and surgical doses of sevoflurane (5%, Figure 5J). Analyses demonstrated that acute propofol exposure led to a lasting

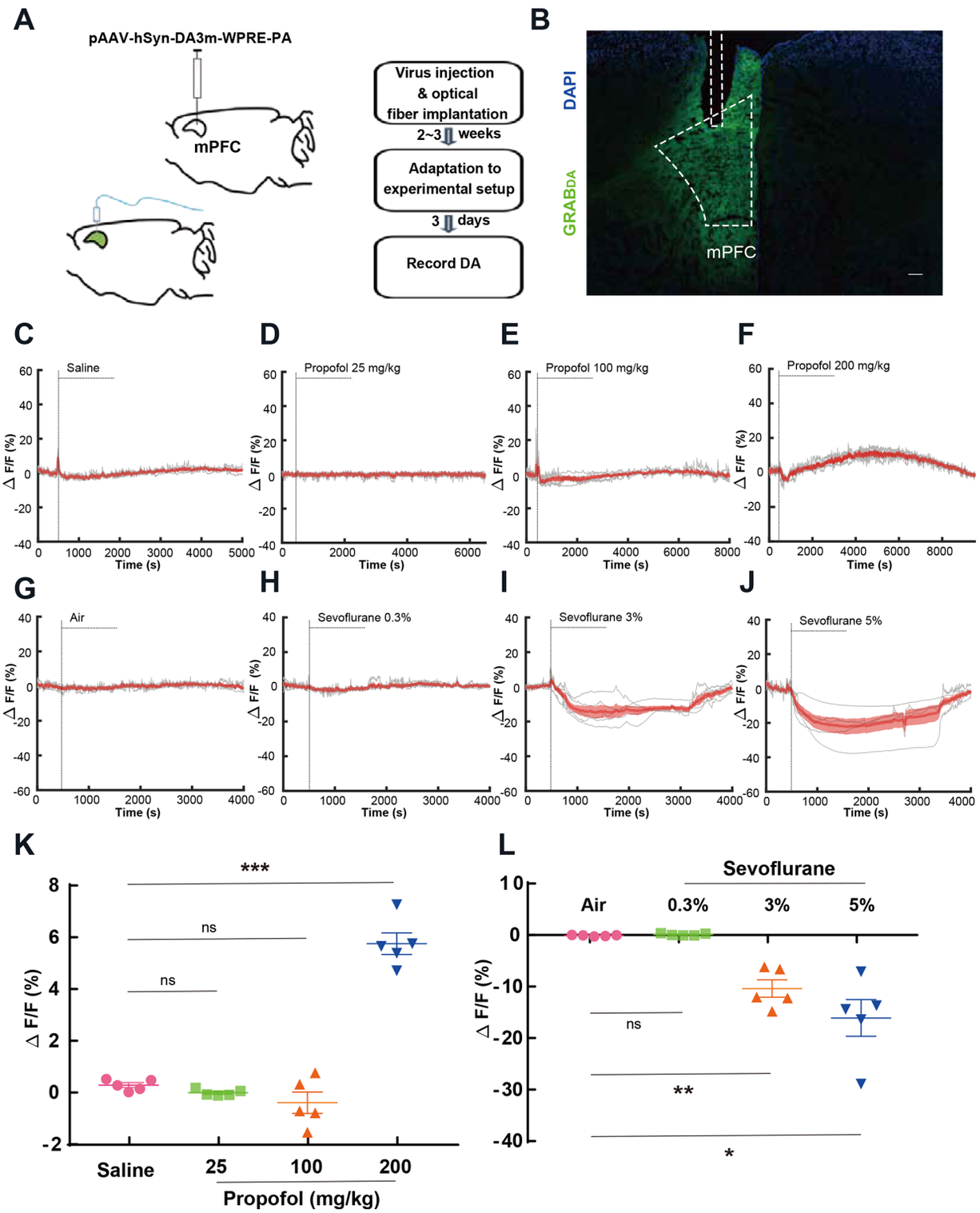

Figure 5 Propofol increases and sevoflurane decreases DA in the mPFC

A: Experimental strategy to record changes in DA signals from mPFC neurons using fiber photometry. B: Representative image displaying DA sensor and fiber channel in the mPFC sample. Scale bar: 200 μm. C−J: DA signals in the mPFC of five mice individually challenged with saline, propofol (25, 100, or 200 mg/kg), air, and sevoflurane (0.3%, 3%, or 5%) administration. Vertical dashed line indicates start of administration. Gray lines depict signals from each mouse, with mean values represented by a red line and SEM intervals shaded in red (n=5 mice). K, L: Statistical results of DA signal changes (one-way ANOVA followed by Dunnett's *post hoc* test; error bars indicate SEM). *: P<0.05; **: P<0.01; ***: P<0.001; ns, not significant.

dose-dependent increase in DA (F=116, P<0.0001, Figure 5K; saline, 0.04 (−0.19; 0.19), median (25%; 75%) vs. propofol, 0.60 (−0.12; 2.25), P=0.22, Supplementary Figure S6E); however, acute sevoflurane exposure led to a significant dose-dependent decrease in DA (F=18.82, P=0.005, Figure 5L; air, 0.02 (−0.50; 0.40), median (25%; 75%) vs. sevoflurane, −12.60 (−15.98; −8.33), P=0.003, Supplementary Figure S6H).

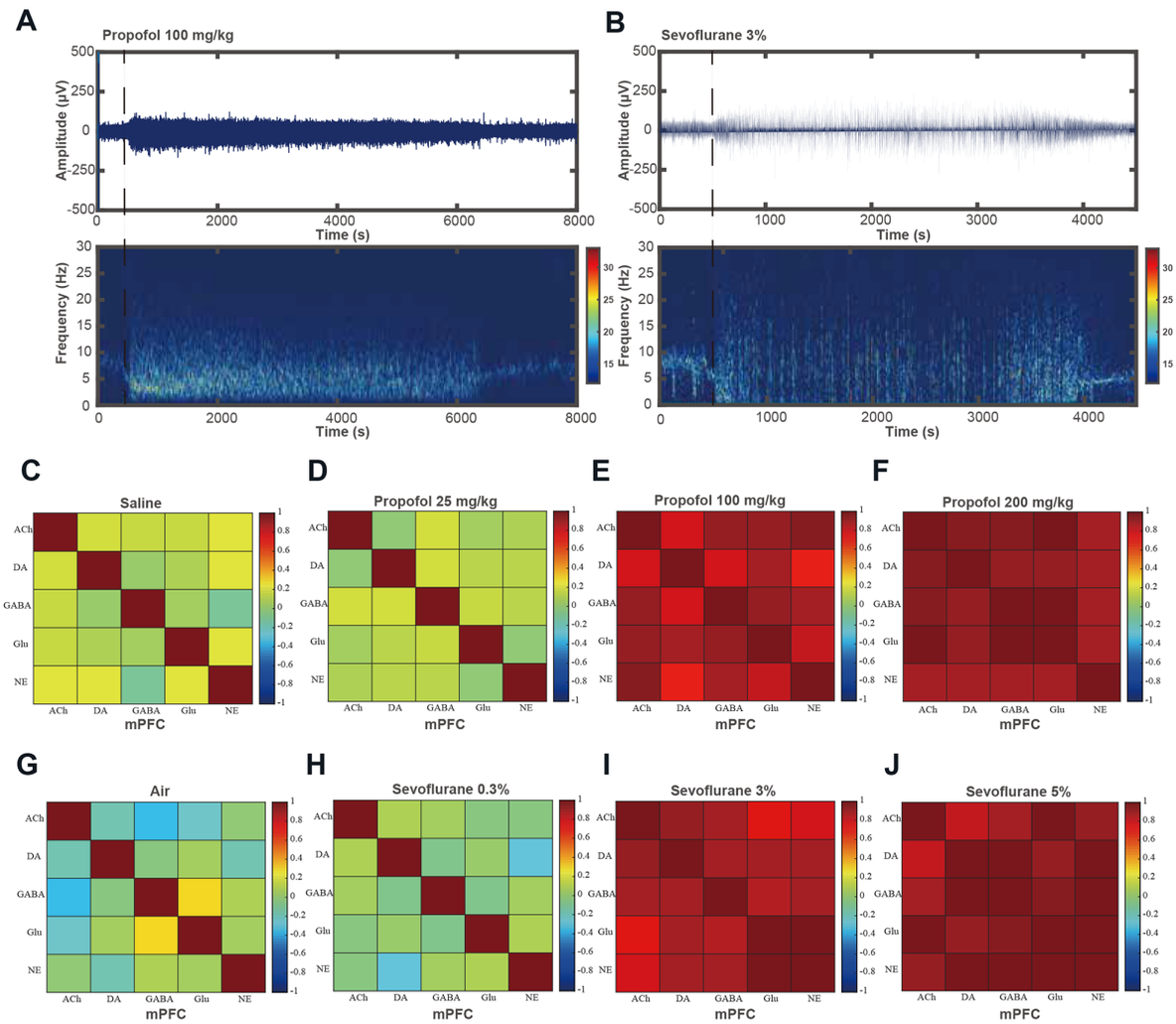

Figure 6 Neurotransmitter dynamic networks synchronize under propofol and sevoflurane anesthesia

A, B: Representative power spectral density of EEG data. Warm colors (e.g., red) represent high power at a given frequency, while cool colors (e.g., blue) represent power. C−J: Heat maps based on Pearson *r* values of neurotransmitter dynamics under saline, propofol (25, 100, or 200 mg/kg), air, and sevoflurane (0.3%, 3%, or 5%) administration. An absolute value of $r>0.4$ indicated high correlation.

Neurotransmitter dynamic networks are synchronized under propofol and sevoflurane anesthesia

As propofol and sevoflurane exerted different effects on different extracellular neurotransmitter dynamics in the mPFC and V1 during aLOC, we were interested in exploring the dynamic networks among neurotransmitters. To better judge the state of consciousness in mice, we performed simultaneous fiber recording and EEG monitoring. According to the EEG results (Figure 6A, B), after hypnotic doses of propofol (time window, 2 000 s) or sevoflurane (time window, 1 000 s), the mice entered a stable aLOC state. We computed the Pearson pairwise correlation coefficients (Pearson's *r*) between neurotransmitter dynamic pairs in the time window of 2 000 s after administration of saline and propofol (25, 100, or 200 mg/kg, Figure 6C−F; Supplementary Figure S7A, B) and the time window of 1 000 s after administration of air or sevoflurane (0.3%, 3%, or 5%, Figure 6G−J; Supplementary Figure S7C, D), with an absolute value of $r>0.4$ defined as a high correlation. Notably, high correlations existed among the neurotransmitter dynamic pairs under both propofol (100 and 200 mg/kg) and sevoflurane (3% and 5%) anesthesia (Figure 6E, F, I, J; Supplementary Figure S7B, D), with the aforementioned doses sufficient to induce LORR in mice. In contrast, low correlations were identified in neurotransmitter dynamic pairs after administration of saline, air, propofol (25 mg/kg), and sevoflurane (0.3%) (Figure 6C, D, G, H; Supplementary Figure S7A, C), with these doses having little apparent effect on the state of consciousness in mice.

DISCUSSION

In this study, we measured the dynamics of five neurotransmitters using *in vivo* fiber photometry and genetically encoded neurotransmitter sensors in the mPFC and V1. The precision of this high spatiotemporal technology, coupled with specific sensors, helped elucidate the dynamics among the five neurotransmitters under propofol and sevoflurane anesthesia. To the best of our knowledge, this study is the first to report that synchronization of neurotransmitter dynamic networks may be a common mechanism of aLOC.

Given the widespread use of propofol as an intravenous general anesthetic (Jiang et al., 2018), we first studied its effects on neurotransmitters in the mPFC and V1. Our findings demonstrated that propofol increased GABA concentration, consistent with the view that general anesthesia inhibits

excitatory synaptic transmission and enhances inhibitory synaptic transmission (Wang et al., 2016; Yang et al., 2019). Notably, our study also showed that the concentrations of DA, Glu, NE, and ACh increased under propofol anesthesia, challenging prevailing perspectives (Gamou et al., 2010; Shirasaka et al., 2011; Zhang et al., 2016). To unravel this unexpected phenomenon, we explored previous studies highlighting the potential of propofol to amplify neurotransmitter levels by inhibiting reuptake mechanisms (Pain et al., 2002; Zhao & Sun, 2008; Zhu et al., 2023). Additionally, propofol, acting as a GABA enhancer, may further contribute to this effect by disinhibiting specific neurons through its action on GABAergic neurons (Gelegen et al., 2018), offering a comprehensive explanation for the elevated neurotransmitter levels observed in the cortex. Our findings provide additional data on the effects of propofol on neurotransmitters in the cortex during aLOC.

As sevoflurane is one of the most common inhaled general anesthetics, we also explored the mechanisms of sevoflurane-induced LOC. Notably, our results showed that sevoflurane decreased both excitatory and inhibitory neurotransmitters, diverging from the impact observed with propofol. The reason for this difference may be that propofol increases the concentration of neurotransmitters primarily by inhibiting the neurotransmitter reuptake process (Pain et al., 2002; Zhao & Sun, 2008), while inhalational anesthetics may reduce neurotransmitter concentrations primarily by inhibiting neurotransmitter release (Baumgart et al., 2015; Speigel et al., 2023).

As different anesthetics exhibit different potencies in inducing anesthesia, it is important to establish equivalent dosages for meaningful comparisons. Thus, we determined the equivalent dosages based on the responses of the mice to the anesthetics. For the low-dose anesthesia group (propofol 25 mg/kg, sevoflurane 0.3%), the mice exhibited a slight sedative response, with no LORR. In contrast, in the hypnotic anesthesia dose group (propofol 100 mg/kg, sevoflurane 3%), the mice responded to painful stimulation and exhibited LORR. In the surgical anesthesia dose group (propofol 200 mg/kg, sevoflurane 5%), the mice displayed minimal response to painful stimulation and experienced LORR. Consequently, our experiment identified dosages of propofol and sevoflurane that are equivalent, although not precisely identical.

The variation in neurotransmitter dynamics induced by propofol and sevoflurane did not prevent LOC, suggesting the potential existence of a shared mechanism underlying these seemingly disparate results. Before administration, the five neurotransmitters maintained a dynamic equilibrium, which persisted after the administration of saline. However, administration of either propofol or sevoflurane disrupted this dynamic balance, leading to a marked increase in synchronization among neurotransmitter dynamics under both anesthetics. Accumulating evidence indicates that cortical activity decreases during LOC, likely due to increases in cortical neuronal synchronization (Akeju et al., 2014; Bharioke et al., 2022; Dasilva et al., 2021; Pazienti et al., 2022). Given the pivotal role of neurotransmitters in mediating the electrical activity of neurons, we hypothesized that the enhanced synchronization of neurotransmitter dynamics induced by general anesthetics may be the mechanism by which aLOC occurs. This theory was verified by our EEG results. EEG signals reflect the overall electrophysiological activity of the cortex. In the awake state, EEG signals are characterized by fast frequency and small amplitude, reflecting complex and inconsistent activity of cortical neurons, resulting in large entropy. Conversely, during the transition from anesthesia induction to maintenance, the EEG signals shist towards lower frequency and increased intensity, corresponding to a reduction in entropy. Our findings indicate that anesthesia induces synchronized alterations in global neurotransmitter levels within the cortex. This synchronization subsequently impacts neuronal excitability, culminating in a cumulative increase in the overall intensity of cortical EEG signals and a decrease in frequency.

Our study has some limitations. Firstly, the exclusive use of male mice may constrain the breadth and interpretation of essential information. Secondly, this study adopted an observational approach, and exploring changes in the depth of anesthesia following interference with neurotransmitter synchronization may provide valuable insights, warranting future exploration. Thirdly, our examination focused on overall neurotransmitter levels; however, the technology employed did not allow for the separation of neurons, synapses, or other structures. Additionally, the underlying causes of the observed neurotransmitter changes remain unclear and require further study. Lastly, other neurotransmitters present but not included in our study merit further attention.

In conclusion, our findings reveal that neurotransmitter dynamic network synchronization may represent a potential mechanism underlying aLOC.

SUPPLEMENTARY DATA

Supplementary data to this article can be found online.

COMPETING INTERESTS

The authors declare that they have no competing interests.

AUTHORS' CONTRIBUTIONS

Study conception: G.L.Q., J.R., and X.S.L.; Study design: G.L.Q., L.J.P., X.S.L., and J.R.; Data acquisition: G.L.Q., L.J.P., P.W., H.L., and X.N.Z.; Data analysis: G.L.Q., L.J.P., Z.L.Y., J.Q.Z., and X.N.Z.; Data interpretation: G.L.Q., L.J.P., P.W., J.R., Z.L.Y., J.Q.Z., X.N.Z., and X.S.L.; Drafting of paper: G.L.Q., L.J.P., J.R., and X.S.L.; Critical revision of paper: all authors. All authors read and approved the final version of the manuscript.

ACKNOWLEDGMENTS

We thank all members of the Key Laboratory of Anesthesiology and Perioperative Medicine of Anhui Higher Education Institutes of Anhui Medical University.

REFERENCES

Akeju O, Westover MB, Pavone KJ, et al. 2014. Effects of sevoflurane and propofol on frontal electroencephalogram power and coherence. *Anesthesiology*, **121**(5): 990–998.

Alkire MT, Gorski LA. 2004. Relative amnesic potency of five inhalational anesthetics follows the Meyer-Overton rule. *Anesthesiology*, **101**(2): 417–429.

Alkire MT, Hudetz AG, Tononi G. 2008. Consciousness and anesthesia. *Science*, **322**(5903): 876–880.

Barttfeld P, Uhrig L, Sitt JD, et al. 2015. Signature of consciousness in the dynamics of resting-state brain activity. *Proceedings of the National Academy of Sciences of the United States of America*, **112**(3): 887–892.

Baumgart JP, Zhou ZY, Hara M, et al. 2015. Isoflurane inhibits synaptic vesicle exocytosis through reduced Ca^{2+} influx, not Ca^{2+}-exocytosis coupling. *Proceedings of the National Academy of Sciences of the United States of America*, **112**(38): 11959–11964.

Bharioke A, Munz M, Brignall A, et al. 2022. General anesthesia globally synchronizes activity selectively in layer 5 cortical pyramidal neurons.

Neuron, **110**(12): 2024–2040. e10.
Carhart-Harris RL, Erritzoe D, Williams T, et al. 2012. Neural correlates of the psychedelic state as determined by fMRI studies with psilocybin. *Proceedings of the National Academy of Sciences of the United States of America*, **109**(6): 2138–2143.
Dasilva M, Camassa A, Navarro-Guzman A, et al. 2021. Modulation of cortical slow oscillations and complexity across anesthesia levels. *NeuroImage*, **224**: 117415.
Feng JS, Zhang CM, Lischinsky JE, et al. 2019. A genetically encoded fluorescent sensor for rapid and specific *in vivo* detection of norepinephrine. *Neuron*, **102**(4): 745–761. e8.
Fornito A, Zalesky A, Breakspear M. 2015. The connectomics of brain disorders. *Nature Reviews Neuroscience*, **16**(3): 159–172.
Gamou S, Fukuda S, Ogura M, et al. 2010. Microinjection of propofol into the perifornical area induces sedation with decreasing cortical acetylcholine release in rats. *Anesthesia & Analgesia*, **111**(2): 395–402.
Gelegen C, Miracca G, Ran MZ, et al. 2018. Excitatory pathways from the lateral habenula enable propofol-induced sedation. *Current Biology*, **28**(4): 580–587. e5.
Guo J, Ran MZ, Gao ZL, et al. 2021. Cell-type-specific imaging of neurotransmission reveals a disrupted excitatory-inhibitory cortical network in isoflurane anaesthesia. *EBioMedicine*, **65**: 103272.
Hemmings Jr HC, Akabas MH, Goldstein PA, et al. 2005. Emerging molecular mechanisms of general anesthetic action. *Trends in Pharmacological Sciences*, **26**(10): 503–510.
Hudetz AG, Mashour GA. 2016. Disconnecting consciousness: is there a common anesthetic end point?. *Anesthesia & Analgesia*, **123**(5): 1228–1240.
Irifune M, Takarada T, Shimizu Y, et al. 2003. Propofol-induced anesthesia in mice is mediated by γ-aminobutyric acid-A and excitatory amino acid receptors. *Anesthesia & Analgesia*, **97**(2): 424–429.
Jiang SF, Liu Y, Huang LN, et al. 2018. Effects of propofol on cancer development and chemotherapy: potential mechanisms. *European Journal of Pharmacology*, **831**: 46–51.
Jing M, Li YX, Zeng JZ, et al. 2020. An optimized acetylcholine sensor for monitoring in vivo cholinergic activity. *Nature Methods*, **17**(11): 1139–1146.
Leon-Dominguez U, Izzetoglu M, Leon-Carrion J, et al. 2014. Molecular concentration of deoxyHb in human prefrontal cortex predicts the emergence and suppression of consciousness. *NeuroImage*, **85**: 616–625.
Liu CX, Zhou X, Zhu QY, et al. 2020. Dopamine neurons in the ventral periaqueductal gray modulate isoflurane anesthesia in rats. *CNS Neuroscience & Therapeutics*, **26**(11): 1121–1133.
Liu H, Wang T, Dai W, et al. 2016. Subhypnotic doses of propofol impair spatial memory retrieval in rats. *Neural Regeneration Research*, **11**(12): 1956–1961.
Luppi AI, Craig MM, Pappas I, et al. 2019. Consciousness-specific dynamic interactions of brain integration and functional diversity. *Nature Communications*, **10**(1): 4616.
Marvin JS, Scholl B, Wilson DE, et al. 2018. Stability, affinity, and chromatic variants of the glutamate sensor iGluSnFR. *Nature Methods*, **15**(11): 936–939.
Marvin JS, Shimoda Y, Magloire V, et al. 2019. A genetically encoded fluorescent sensor for in vivo imaging of GABA. *Nature Methods*, **16**(8): 763–770.
McGovern DJ, Polter AM, Root DH. 2021. Neurochemical signaling of reward and aversion to ventral tegmental area glutamate neurons. *Journal of Neuroscience*, **41**(25): 5471–5486.
Meyer K. 2015. The role of dendritic signaling in the anesthetic suppression of consciousness. *Anesthesiology*, **122**(6): 1415–1431.
Müller CP, Pum ME, Amato D, et al. 2011. The *in vivo* neurochemistry of the brain during general anesthesia. *Journal of Neurochemistry*, **119**(3): 419–446.
Nishino T, Jin H, Nozaki-Taguchi N, et al. 2020. A high concentration of sevoflurane induces gasping breaths in mice. *Respiratory Physiology & Neurobiology*, **279**: 103445.
Pain L, Gobaille S, Schleef C, et al. 2002. *In vivo* dopamine measurements in the nucleus accumbens after nonanesthetic and anesthetic doses of propofol in rats. *Anesthesia & Analgesia*, **95**(4): 915–919.
Patel S, Wohlfeil ER, Rademacher DJ, et al. 2003. The general anesthetic propofol increases brain N-arachidonylethanolamine (anandamide) content and inhibits fatty acid amide hydrolase. *British Journal of Pharmacology*, **139**(5): 1005–1013.
Pazienti A, Galluzzi A, Dasilva M, et al. 2022. Slow waves form expanding, memory-rich mesostates steered by local excitability in fading anesthesia. *Iscience*, **25**(3): 103918.
Qiu GL, Wu Y, Yang ZY, et al. 2020. Dexmedetomidine activation of dopamine neurons in the ventral tegmental area attenuates the depth of sedation in mice. *Anesthesiology*, **133**(2): 377–392.
Rose J, Weiser TG, Hider P, et al. 2015. Estimated need for surgery worldwide based on prevalence of diseases: a modelling strategy for the WHO Global Health Estimate. *The Lancet Global Health*, **3**(Suppl 2): S13–S20.
Shirasaka T, Yonaha T, Onizuka S, et al. 2011. Effects of orexin-A on propofol anesthesia in rats. *Journal of Anesthesia*, **25**(1): 65–71.
Silva S, De Pasquale F, Vuillaume C, et al. 2015. Disruption of posteromedial large-scale neural communication predicts recovery from coma. *Neurology*, **85**(23): 2036–2044.
Smith JB, Liang ZF, Watson GDR, et al. 2017. Interhemispheric resting-state functional connectivity of the claustrum in the awake and anesthetized states. *Brain Structure and Function*, **222**(5): 2041–2058.
Speigel I, Patel K, Osman V, et al. 2023. Volatile anesthetics inhibit presynaptic cGMP signaling to depress presynaptic excitability in rat hippocampal neurons. *Neuropharmacology*, **240**: 109705.
Sun FM, Zeng JZ, Jing M, et al. 2018. A genetically encoded fluorescent sensor enables rapid and specific detection of dopamine in flies, fish, and mice. *Cell*, **174**(2): 481–496. e19.
Sun FM, Zhou JH, Dai B, et al. 2020. Next-generation GRAB sensors for monitoring dopaminergic activity in vivo. *Nature Methods*, **17**(11): 1156–1166.
Supp GG, Siegel M, Hipp JF, et al. 2011. Cortical hypersynchrony predicts breakdown of sensory processing during loss of consciousness. *Current Biology*, **21**(23): 1988–1993.
Wang H, Jing M, Li YL. 2018. Lighting up the brain: genetically encoded fluorescent sensors for imaging neurotransmitters and neuromodulators. *Current Opinion in Neurobiology*, **50**: 171–178.
Wang Y, Yu T, Yuan CD, et al. 2016. Effects of propofol on the dopamine, metabolites and GABAA receptors in media prefrontal cortex in freely moving rats. *American Journal of Translational Research*, **8**(5): 2301–2308.
Xu P, Chen A, Li YP, et al. 2019. Medial prefrontal cortex in neurological diseases. *Physiological Genomics*, **51**(9): 432–442.
Yang J, Wang W, Yong Z, et al. 2019. Propofol inhibits the local activity and connectivity of nuclei in the cortico-reticulo-thalamic loop in rats. *Journal of Anesthesia*, **33**(5): 572–578.
Zhang LL, Jin J, Yao JY, et al. 2016. Effects of propofol on excitatory and inhibitory amino acid neurotransmitter balance in rats with neurogenic pulmonary edema induced by subarachnoid hemorrhage. *Neurocritical Care*, **24**(3): 459–471.
Zhao YJ, Sun LN. 2008. Antidepressants modulate the *in vitro* inhibitory effects of propofol and ketamine on norepinephrine and serotonin transporter function. *Journal of Clinical Neuroscience*, **15**(11): 1264–1269.
Zheng J, Li HL, Tian N, et al. 2020. Interneuron accumulation of phosphorylated tau impairs adult hippocampal neurogenesis by suppressing GABAergic transmission. *Cell Stem Cell*, **26**(3): 331–345. e6.
Zhou C, Liang P, Liu J, et al. 2015. HCN1 channels contribute to the effects of amnesia and hypnosis but not immobility of volatile anesthetics. *Anesthesia & Analgesia*, **121**(3): 661–666.
Zhu XN, Li J, Qiu GL, et al. 2023. Propofol exerts anti-anhedonia effects via inhibiting the dopamine transporter. *Neuron*, **111**(10): 1626–1636. e6.